Effect of Sheath Structure on Operating Stability in an Anode Layer Thruster

Shinsuke YASUI, Naoji YAMAMOTO*, Kimiya KOMURASAKI**, and Yoshihiro ARAKAWA**
University of Tokyo, Tokyo 113-8656, JAPAN
** Department of Aeronautics and Astronautics*
*** Department of Advanced Energy*
Email: yasui@al.t.u-tokyo.ac.jp

Keywords: Electric Propulsion, Hall Thruster, Hollow Anode

Abstract

The discharge current oscillation has been measured for various hollow anode widths and its axial positions using a 1kW-class anode layer hall thruster. As a result, there were thresholds of magnetic flux density for stable discharge. The plasma structure inside the hollow anode was numerically analyzed using the fully kinetic 2D3V Particle-in-Cell (PIC) and Direct Simulation Monte Carlo (DSMC) methods. The results reproduced both stable and unstable operation modes. In the stable operation case, which corresponds to the case with low magnetic flux, the plasma penetrated into the hollow anode deeper than the case with higher magnetic flux density case. This suggests that comparably large substantial anode area should contribute to stable operation.

Introduction

Discharge instability in anode layer hall thrusters would be one of the serious problems to be overcome. A hollow anode is commonly used to stabilize the discharge for these thrusters.[1-3] However, its mechanism has not been clarified yet and optimization has not been done.

In this research, the mechanism of discharge stabilization using a hollow anode was investigated experimentally and analytically. The goal of the study is to model the anode sheath, which has a great effect on the stable discharge of anode layer hall thrusters, and find out a scaling law for the anode design.

In the experimental study, a 1kW-class anode layer hall thruster with a hollow anode has been designed and fabricated in university of Tokyo.[4] Discharge current oscillation has been measured for various hollow widths and its axial positions.

As for the computational study, the structure of electrical sheath inside a hollow anode was numerically simulated using the fully kinetic 2D3V Particle-in-Cell (PIC) and Direct Simulation Monte Carlo (DSMC) methodologies.[5-8]

Experiment

Anode Layer Hall Thruster

The cross section of thruster is shown in Fig. 1. It has two guard rings made of stainless steel. They are kept at the cathode potential. The inner and outer diameters of an acceleration channel are 48mm and 62mm, respectively. A solenoidal coil is set at the center of the thruster to apply radial magnetic field in the acceleration channel. Magnetic flux density is variable by changing coil current. As an electron source, a filament cathode (2% thoriated tungsten of ϕ 0.27mm × 500mm × 3) was used to minimize discharge fluctuations originated from cathode operation instability.

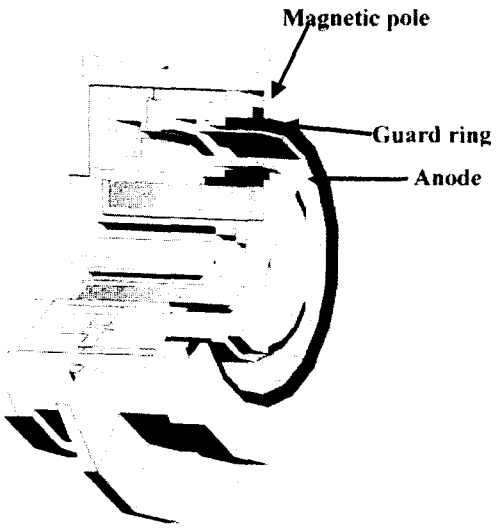

Fig. 1 The cross section of the thruster.

Operating and Geometric Parameters

It has an annular hollow anode made of cupper. We defined Z as the distance between the thruster exit and the tip of anode, and D as the width of anode channel as indicated in Fig. 2. Z and D are varied (Z=1-4mm, D=1-3mm) in this study. Xenon was used as a propellant, and the mass flow rate was set at $1.0A_{eq}$=1.37mg/s. Discharge voltage was set at 400V. Under these conditions, the amplitude of discharge current oscillation has been measured for various magnetic flux densities.

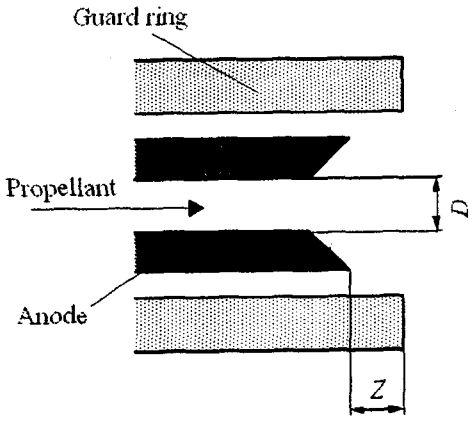

Fig. 2 Definitions of Z and D.

Discharge Current Oscillation

Figure 3 shows measured amplitude of discharge current oscillation and the time-averaged discharge current $\overline{I_d}$. Here, the amplitude of discharge current oscillation is defined as,

$$\sqrt{\frac{\int_0^\tau (I_d - \overline{I_d})^2}{\tau}} \Big/ \overline{I_d} \qquad (1)$$

Oscillation amplitude was sensitive to magnetic flux density B. Although the oscillation was small at B<0.014T, the thrust efficiency was poor in this range of B because of large electron backflow current. Therefore, the desirable operation condition was limited in a quite narrow range of B.

Table 1 shows the sensitivity of discharge stability to the geometric parameters Z and D. The cases when oscillation amplitude didn't go down to 0.1 for any B are defined "unstable." Typically, stable discharge has not been realized with small Z and small D.

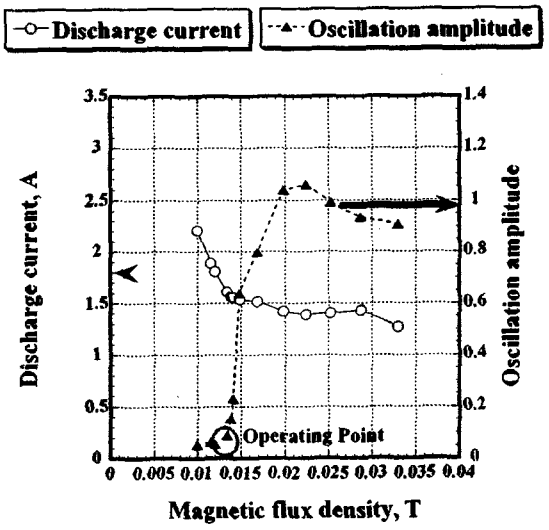

Fig. 3 Oscillation characteristics. D=3mm, Z=1mm.

Table 1 Discharge stability for various D and Z.

D[mm] \ Z[mm]	1	2	3	4
1	×	×	○	○
2	×	○	○	○
3	○	○	○	○

○ : Stable ×: Unstable.

Measured oscillation amplitude is plotted for various geometries in Fig. 4. There was a common trend that operation becomes unstable with the increase in B as seen in Fig. 3. The threshold of B was about 0.011-0.015T.

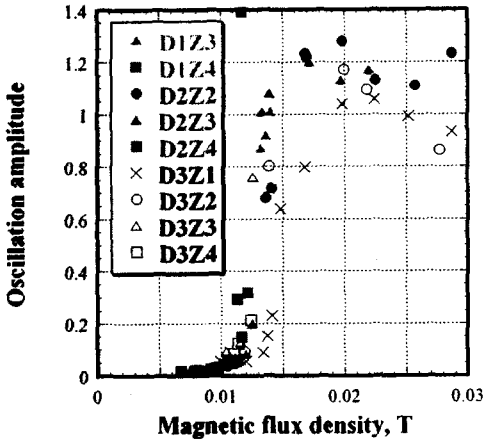

Fig. 4 Relation between oscillation amplitude and B. Z=1-4mm, D=1-3mm.

Calculation

Computational Methods and Physical Models

It is very difficult to measure the distributions of electric potential and plasma density inside a hollow anode. The structure of electrical sheath inside the hollow anode was numerically computed using the fully kinetic 2D3V Particle-in-Cell (PIC) and Direct Simulation Monte Carlo (DSMC) methodologies. Figure 5 shows the flow chart of this calculation.

10^6-10^9 of real particles were treated as one macro particle and all of macro particles were treated kinetically. Electric and magnetic forces were implemented via the PIC method and collisions were via the DSMC method. The cylindrical coordinate system (r, z, θ) was applied to the region inside the hollow anode as shown in Fig. 6. Particle's position is expressed in two-dimensional space r and z, while its velocity is expressed in three-dimensional space. That is, particles move in all directions, but the azimuthal coordinate is always discarded.

An orthogonal calculation grid was set, with the axial length of the cell getting smaller toward the anode exit in order to observe the sharp fall of

electron density in the vicinity of anode exit. The minimum cell length is in the same order of the Debye length.

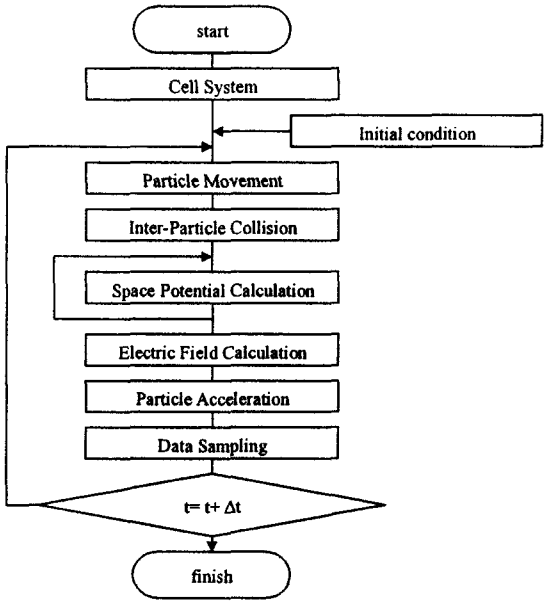

Fig. 5 A flow chart of the calculation.

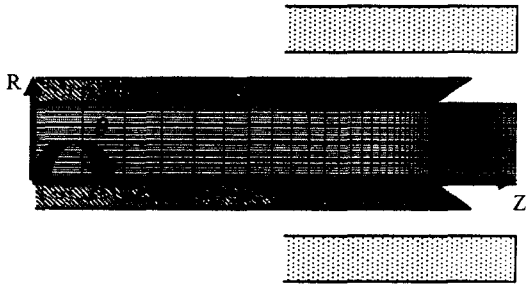

Fig. 6 The coordinate and the calculation grid.

Assumptions are listed below.

Magnetic field lines are aligned in the radial direction and don't have axial or azimuthal components. Figure 7 shows the assumed magnetic flux density distribution in the calculation. B_0 is variable.

Only singly charged ionization is considered.

Mass ratio m_e/m_n is decreased from 4×10^{-6} to 1/100, to slow down electron's motion. It allows time step to rough and speeds up the calculation.

Potential difference between anode and plasma at the thruster exit boundary is set at 250V.

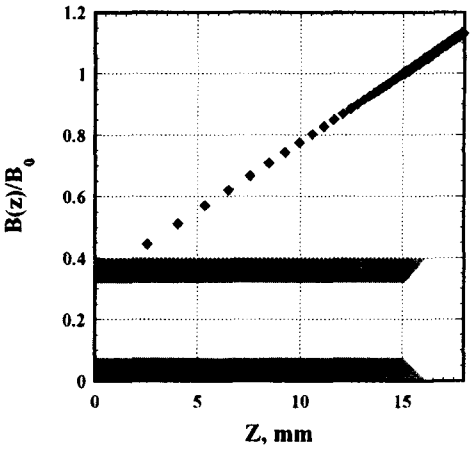

Fig. 7 Assumed magnetic flux density distribution in the calculation.

Propellant mass flow rate was set at $0.5A_{eq}$. Electrons were fed from the anode exit with a T_e=10eV half-Maxwellian velocity distribution.

Collisions considered in this simulation are shown in Table 2. The mean free time and collision frequency in the table are typical values when the particles are at their thermal velocity. We considered three dominant collisions; electron-neutral scattering, ionization, excitation. The simulation time step (typically 1.22×10^{-11}s) was set based on Larmor frequency, and that is much smaller than electron-neutral collision mean free time.

Table 2 Collisions considered in the simulation.

Collision	Mean Free Time, s	Relative Collision Frequency
Electron–Neutral Elastic Scattering	2.038×10^{-9}	1.00
Electron–Neutral Ionization	1.831×10^{-8}	0.111
Electron–Neutral Excitation	6.683×10^{-8}	3.05×10^{-2}
Electron–Ion Coulomb	2.827×10^{-7}	7.21×10^{-3}
Electron–Electron Coulomb	1.527×10-5	1.33×10-4
Neutral–Neutral Scattering	3.83×10-5	5.32×10-5

All the particles moved according to the dynamic equations. The dynamic equations for charged particles are expressed as,

$$\text{Electrons:}\begin{cases} m_e\dfrac{dv_Z}{dt} = -e(E_Z - v_\theta B_R) \\ m_e\dfrac{dv_R}{dt} = -eE_r + m_e\dfrac{v_\theta^2}{x_R} \\ m_e\dfrac{dv_\theta}{dt} = -ev_Z B_R - m_e\dfrac{v_R v_\theta}{x_R} \\ \dfrac{dx_Z}{dt} = v_z, \quad \dfrac{dx_R}{dt} = v_R \end{cases} \tag{2}$$

$$\text{Ions :}\begin{cases} m_i\dfrac{dv_Z}{dt} = eE_Z \\ m_i\dfrac{dv_R}{dt} = eE_R \\ \dfrac{dx_Z}{dt} = v_Z \\ \dfrac{dx_R}{dt} = v_R \end{cases} \tag{3}$$

Space potential was calculated using the Poisson's equation as,

$$\frac{\partial^2\varphi}{\partial Z^2} + \frac{1}{x_R}\frac{\partial}{\partial R}\left(x_R\frac{\partial\varphi}{\partial R}\right) = -\frac{e}{\varepsilon_0}(n_i - n_e) \tag{4}$$

Results and Discussions

Figure 8 shows the calculated discharge current histories. Discharge was stable in the case of B_0=0.01T. Discharge current was 0.33A, oscillation amplitude was 0.01, and ion current was 0.14A (propellant utilization efficiency η_u=28%). On the other hand, discharge oscillation was observed in the case of B_0=0.03T. Oscillation frequency(~100kHz) was on the same order with experimental one. Averaged discharge current was 0.15A, oscillation amplitude was 0.10, and ion current was 0.12A (η_u=24%).

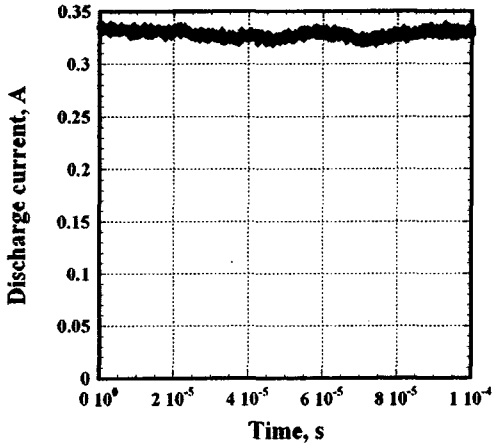

(a) B_0=0.01T.

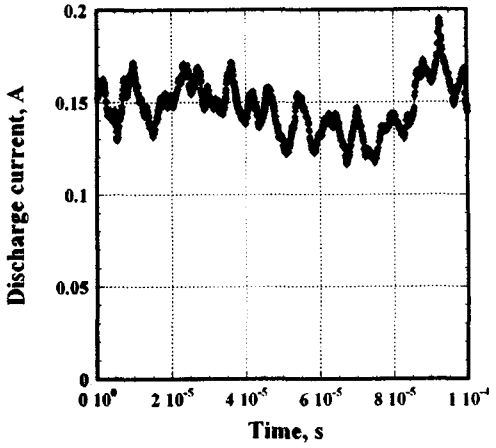

(b) B_0=0.03T.

Fig. 8 Calculated discharge current histories. Z=3mm, D=3mm.

Discharge current was smaller with higher magnetic flux density, similar to the experimental results.

Computed distributions of electron number density are shown in Fig. 9. In the case of B_0=0.01T, plasma has penetrated deeply into the anode channel. Therefore, substantial anode surface area that contacts the plasma is large. Then, the hollow anode would be able to absorb electrons smoothly without a large sheath drop.

When B_0=0.03T, plasma less penetrated into the anode channel, and substantial anode surface area is small compared with the case B_0=0.01T.

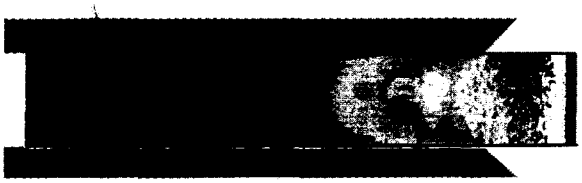

(a) B_0=0.01T.

(b) B_0=0.03T.

Fig. 9 Computed electron number density distributions.
Contour max 1.0×10^{18}m^{-3}, min 0.1×10^{18}m^{-3}.

Figure 10 shows current density distribution on the anode surface. In the case of B_0=0.03T, most electrons have flew into near the anode exit region, while electron density was small in this region. This resulted in large sheath drop on the anode surface.

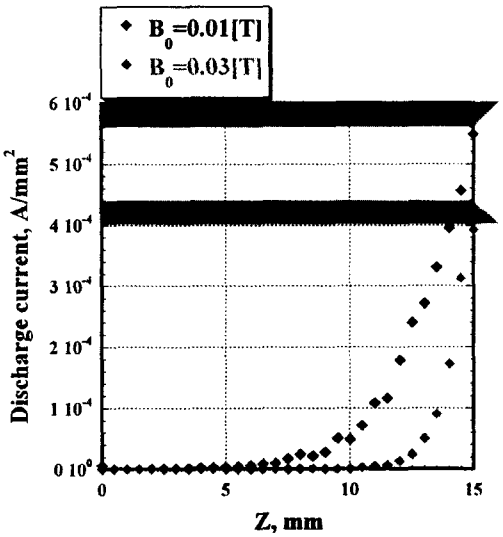

Fig. 10 Current density distribution on the anode surface.

Figure 11 shows the computed space potential distributions. There existed a positive sheath drop at the edge of anode exit in the case of B_0=0.03T. This might be a reason of discharge instability.

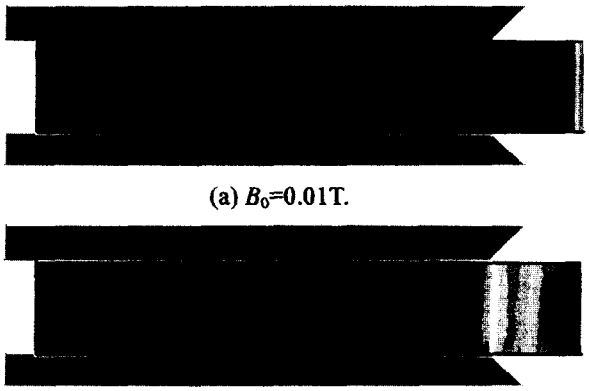

(a) B_0=0.01T.

(b) B_0=0.03T.

Fig. 11 Computed electric potential distributions. Contour max 250V, min 0V.

For the validation of computation, the measured potential distribution[9] is shown in Fig. 12. (Discharge voltage was 250V). The potential increases sharply in the vicinity or the outside of the thruster exit for the case of small B_0. As B_0 is getting larger, potential gradient becomes slower. These experimental trends well agreed with the calculation ones.

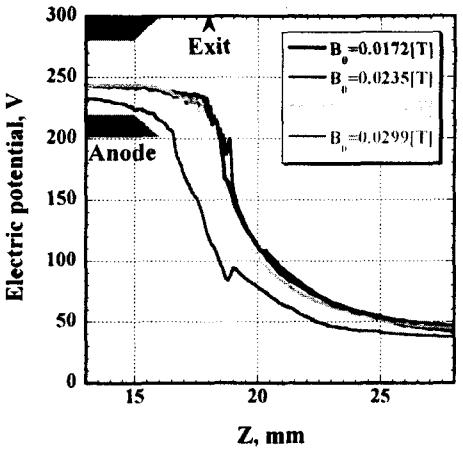

Fig. 12 Electric potential measured in experiment.

Conclusions

In the experiment, it was found that there were thresholds of magnetic flux density for stable discharge. The computed sheath structure inside a hollow anode suggested that large substantial anode surface area created by a hollow anode should contribute to the stabilization of discharge.

References

1) Choueiri, E. Y., "Fundamental difference between the two Hall thruster variants", Physics of Plasmas Vol.8, No.11 November 2001.
2) Semenkin A.V., Tverdokhlebov S.O., Garkusha V.I., Kochergin A.V., Chislov G.O., Shumkin B.V., Solodukhin A.V., Zakharenkov L.E., "Operating Envelopes of Thrusters with Anode Layer", IEPC2001-013, 27th International Electric Propulsion Conference, Pasadena, USA, October 2001.
3) Semenkin, A., Kochergin, A., Garkusha, V., Chislov, G., Rusakov, A., "RHETT/EPDM Flight Anode Layer Thruster Development", IEPC-97-106, 25th International Electric Propulsion Conference, Cleveland, USA, August 1997.
4) Yamamoto, N., Nakagawa, T., Komurasaki, K., Arakawa, Y., "Extending Stable Operation Range in Hall Thrusters", AIAA-2002-3953 38th AIAA/ASME/SAE/ASEE Joint Propulsion Conference & Exhibit, Indianapolis, USA, July 2002.
5) Hirakawa, M., "Particle Simulation of Plasma Phenomena in Hall Thrusters", IEPC-95-164, 24th International Electric Propulsion Conference, Moscow, Russia, September 1995.
6) Szabo, J. J., "Fully Kinetic Hall Thruster Modeling", IEPC-01-341, 27th International Electric Propulsion Conference, Pasadena, USA,

October 2001.
7) Szabo, J. J., "Fully Kinetic Hall Thruster Modeling of a Plasma Thruster", PhD Thesis, Massachusetts Institute of Technology, 2001.
8) Szabo, J., Rostler, P., "One and Two Dimensional Modeling of the BHT-1000", IEPC-02-231, 28th International Electric Propulsion Conference, Toulouse, France, March 2003.
9) Yamamoto, N., Nakagawa, T., Komurasaki, K., Arakawa, Y., "Effect of Discharge Oscillations on Hall Thruster Performance", ISTS 2002-b-17, 23rd the International Symposium on Space Technology and Science, Shimane, Japan, May 2002.

Appendix

Nomenclature

B: magnetic induction
D: anode hollow width
e: electronic charge
E: electric field strength
I_d: discharge current
m: particle mass
n: number density
t: time
T: temperature
v: velocity
x: position
Z: distance between anode tip and channel exit
ε_0: free space permeability
φ: space potential
η_u: propellant utility efficiency
r, z, θ: cylindrical coordinate

Subscripts

0: anode exit
e: electron
i: ion
n: neutral